Ganoderma lucidum polysaccharides improve liver metabolic disorders by modulating gut microbiota of ovariectomized mice

XIN JIN[1*], XUAN LIU[2*], YUN-JUAN WANG[1], ZI-LI LEI[2] and YAN-HONG YANG[1]

[1]The First Affiliated Hospital (The First School of Clinical Medicine), Guangdong Pharmaceutical University, Guangzhou, Guangdong 510080, P.R. China; [2]Guangdong Metabolic Diseases Research Center of Integrated Chinese and Western Medicine, Guangdong Pharmaceutical University, Guangzhou Higher Education Mega Center, Guangzhou, Guangdong 510006, P.R. China

Received December 10, 2025; Accepted April 28, 2026

DOI: 10.3892/ijmm.2026.5866

Abstract. The morbidity of cardiovascular disease in postmenopausal patients increases due to the lack of estrogen protection. One of the most common conditions is hyperlipidemia characterized by abnormally elevated low-density lipoprotein cholesterol (LDL-C) and total cholesterol (TC). GLP has multiple effects such as lowering lipid levels, reducing inflammation, and regulating gut microbiota, but its effect on regulating metabolism in menopausal patients is not clear. The present study aimed to study the regulatory effect of *Ganoderma lucidum* polysaccharides (GLPs) on cholesterol metabolism in the liver. A bilateral ovariectomy mouse model was generated and GLP was given by gavage. Serum biochemistry, hepatic architecture and histopathology were assessed, expression of genes governing glucose and lipid homeostasis and circadian rhythm in the hepatic tissue was detected and the changes of intestinal microbiota of ovariectomized mice was analyzed by 16S rDNA sequencing. The GLPs directly affected the intestinal flora, upregulated the abundance of probiotics and improved the structure of microbiota and might indirectly affect the liver metabolism through the gut-liver axis. GLP administration markedly lowered circulating TC and LDL-C, decreased hepatic steatosis and modulated the expression of genes associated with the circadian clock, lipid synthesis and glucose metabolism in hepatic tissue. Collectively, these data position GLP as a promising therapeutic candidate for correcting postmenopausal dysmetabolism and curbing cardiovascular risk in aging female patients.

Correspondence to: Professor Yan-Hong Yang, The First Affiliated Hospital (The First School of Clinical Medicine), Guangdong Pharmaceutical University, 19 Nong-Lin-Xia Road, Yue-Xiu, Guangzhou, Guangdong 510080, P.R. China
E-mail: 1764941457@qq.com

Dr Zi-Li Lei, Guangdong Metabolic Diseases Research Center of Integrated Chinese and Western Medicine, Guangdong Pharmaceutical University, Guangzhou Higher Education Mega Center, 280 Wai Huan Dong Road, Guangzhou, Guangdong 510006, P.R. China
E-mail: 3182683090@qq.com

*Contributed equally

Key words: ovariectomy, *Ganoderma lucidum* polysaccharide, circadian rhythm, lipid metabolism, gut microbiota

Introduction

Following menopause, the risk of cardiovascular disease (CVD) rises sharply compared with that in younger patients, making it the primary cause of death in elderly female patients (1,2). Patients who transition through menopause at an age less than 45 years are at a 50% increased CVD risk and they also have a 10% increased risk of fatal coronary heart disease and all-cause mortality (1). In these patients, hyperlipidemia, characterized by abnormally elevated LDL-C and TC, is common (3,4). HDL-C levels are not associated with menopause status, but higher LDL-C, TG, and TC levels are observed in postmenopausal than in premenopausal women (3). Patients who experienced natural menopause were at 3-times greater risk of atherosclerosis compared with premenopausal patients and menopause is a risk factor for age-related increase in arterial stiffness (5). Another peer study also showed a higher rate of CVD events in postmenopausal patients (6). Age at menopause is not only a sign of reproductive aging, but also a high-risk indicator of CVD (7). In addition, the decline of ovarian function and the decrease in estrogen can lead to physical and psychological symptoms in older patients, including osteoporosis, cognitive decline, night sweats, hot flashes, insomnia, depression and metabolic abnormality (8,9). These factors have a serious impact on the life and health of elderly patients. Hormone therapy is commonly used for postmenopausal patients at high risk of CVD, but studies have reported that the disadvantages of hormone therapy may outweigh the benefits and that the efficacy of treatment is influenced by factors such as dosage used, mode of administration and time of menopause (10,11). Consequently, devising safer and more efficacious therapy for preventing and treating dyslipidemia associated with menopause is important.

Polysaccharides can ameliorate metabolic dysfunction-associated steatotic liver disease (MASLD), type 2 diabetes and obesity by modulating lipid metabolism, suppressing inflammation, scavenging free radicals and reshaping the gut

microbiota (12-14). For example, hawthorn polysaccharides significantly ameliorate high-fat diet (HFD)-induced MASLD by modulating the gut microbiota and ameliorating metabolic disorders in the liver of mice (15). *Ganoderma lucidum* has been employed medicinally in China and across much of Asia (16). *G. lucidum* polysaccharides (GLPs), the primary bioactive constituent, have demonstrated antitumor (17), antioxidant, immunomodulatory and lipid-metabolism-modulating activity (18). *G. lucidum* β-D-glucan forms a hydrogen-bonded stable triple helix structure and its biological activity depends on the β configuration (18). Differences in separation methods and culture media lead to a diverse structure of polysaccharides, including pure β-glucan, isosaccharides, heteromannans and their peptide complexes (19). In different animal models, GLP can induce the synthesis of superoxide dismutase, succinate dehydrogenase and glutathione (GSH) and decrease levels of TC, triglyceride (TG) and LDL-C, thereby decreasing hyperlipidemia (18,20,21). GLP regulates glucose metabolism, such as downregulating serum glucose and insulin (INS) levels, inhibiting β cell apoptosis and promoting the regeneration of β cells (22,23). In addition, GLP modulates intestinal dysbiosis: In mice exposed to azoxymethane/dextran sulfate sodium, GLP suppresses colitis, inflammation and tumorigenesis, and simultaneously corrects microbial imbalances while alleviating endotoxemia (24). In diabetic rats, GLP lowers inflammation and enriches beneficial gut microbes, thereby bolstering host defense against pathogens (25). Hence, investigating how GLP ameliorates metabolic disorders in postmenopausal patients along with its underlying mechanisms is imperative.

There is a connection between intestinal flora and estrogen: A specific part of the intestinal flora uses β-glucosidase to convert the bound form of estrogen into a free, active state, which binds receptors and exerts effects, such as stimulating the development of ovarian follicles, enhancing bone density and providing cardiovascular protection (26,27). In postmenopausal patients, the composition and quantity of intestinal microbiota change, which may also be one of the mechanisms of metabolic disorders (28). Patients experiencing menopausal vasomotor disorders tend to have a notable decline in the primary representatives of *Bifidobacterium* and *Lactobacillus*, meanwhile, there is an increase in the quantities of *Klebsiella* and *Clostridioides* difficile (29,30). On the other hand, the liver, as the hub of material metabolism, plays a key role in regulating metabolism, including regulating the synthesis and metabolism of lipids, sugar and proteins (31). A large number of clinical studies support the role of gut microbiota in liver disease and an imbalanced gut microbiota affects the metabolic and inflammatory state of the liver, which affects the disease process, including hepatocellular carcinoma, hepatitis and liver cirrhosis (32,33). Polysaccharides derived from *G. lucidum* spores curb obesity and inflammation while attenuating hyperlipidemia through modulation of the gut microbiota (24). Therefore, based on the gut-liver axis theory, although GLP is not easily absorbed by the intestine, it may regulate liver metabolism by affecting the intestinal flora, thereby improving metabolic disorder.

The present study used a mouse model of ovariectomy to simulate ovarian hormone deficiency in elderly female patients and explored the regulatory effect and molecular mechanism of GLP on body weight, liver lipids, circadian rhythm, INS resistance and intestinal microbiota, providing a theoretical basis for the potential use of GLP in the treatment of lipid metabolic disorder of postmenopausal patients.

Materials and methods

Animal experiments. All the animal experiments were approved by the Experimental Animal Ethics Committee of Guangdong Pharmaceutical University (Guangzhou, China; approval no. gdpulac2020065) and adhered to ARRIVE2 (34). In total, 72 female C57BL/6 mice (weight, 17-19 g; age, 7 weeks) purchased from Hunan Lex Jingda Laboratory Animal Co., Ltd. were housed in a specific pathogen-free animal facility at 25˚C, 60-65% humidity, 12/12-h light/dark cycle, with free access to water and food. To observe the anesthetic concentration and postoperative condition of the mice, three mice were randomly selected, two for ovariectomy and one for sham surgery. This was repeated once/day for 3 consecutive days, confirming that a 3% isoflurane anesthetic concentration was suitable for surgery and that the mice were in good condition after the operation. Following 1 week of adaptive feeding, mice were randomized and 63 mice were used for the subsequent experiments. Groups were as follows: Sham operation (n=10); bilateral ovariectomy (OVX, n=11); OVX + low-dose (100 mg/kg) GLP (OVX + LGLP, n=11); OVX + medium-dose (200 mg/kg) GLP (OVX + MGLP, n=10); OVX + high-dose (400 mg/kg) GLP (OVX + HGLP, n=10) and OVX + simvastatin (Siv; 10 mg/kg; n=11). Siv was chosen as the positive reference drug. Mice were placed in an induction chamber with 3% isoflurane in oxygen for anesthesia induction. Following loss of consciousness, animals were maintained with 2% isoflurane for bilateral ovariectomy. For the sham operation group, ovaries were removed and replaced, with all other procedures identical to the ovariectomy group. GLP (cat. no. Ksm083, Ciyuan Biotechnology) was dissolved in sterile water and given once daily by gavage. Every afternoon at 2.00, after weighing the mice in each group, gavage was performed. Sham group and OVX group mice were gavaged with the corresponding volume of sterile water. The body weight of the mice was measured daily. Humane endpoints were as follows: Weight loss >20%, complete refusal to eat/drink for 24 h, inability to stand for 48 h, severe depression/coma, uncontrollable infection or severe respiratory distress. Animals were monitored once daily. A total of 63 animals were used; no animals reached these humane endpoints, and all animals were euthanized at the planned experimental endpoints. Following 8 weeks of gavage, the mice were fasted for 8 h. Animals were induced and maintained with 3% isoflurane in oxygen until loss of consciousness (absent righting reflex) and absent toe pinch reflex. Animals were maintained at 3% isoflurane for 3-5 min for deep anesthesia. Terminal blood collection (0.8-1.0 ml, ≤50% of total blood volume) was performed via retro-orbital sinus puncture using heparinized capillary tubes. Immediately after blood collection, mice were euthanized by cervical dislocation while under anesthesia. Death was confirmed by cessation of heartbeat and respiratory arrest. Liver tissue was collected for biochemical, histological and transcriptional testing. Stool samples of the mice were collected in the last week of the experimental process and frozen at -80˚C.

GLP characterization. The monosaccharide composition was determined by high performance anion electronic chromatography (HPAEC) with electrochemical detectors (EDs). In brief, GLP (5 mg) was added to 3 M trifluoroacetic acid. After that, the solution was heated for 3 h at 120˚C. The hydrolyzed products were thoroughly dissolved in 5 ml ddH_2O with a vortex, then, 50 μl liquid was diluted with 950 μl ddH_2O. The solution was centrifuged at a rate of 13,400 x g for 5 min at room temperature. A membrane with a 0.22 μm pore size was used to filter the supernatant before examination with an HPAEC-ED fitted with a Dionex Carbopac PA20 column (Thermo Fisher Scientific, 150.0x3.0 mm). The mobile phase elution was performed at the flow rate of 0.3 ml/min using the following mobile phase: A, H_2O; B, 15 mM NaOH; and C, 15 mM NaOH and 100 mM NaOAc. The injection volume was 25 μl and the column temperature was 30˚C. Elution gradient was performed as follows: 0 min A/B/C (98.8:1.2:0.0), 18 min A/B/C (98.8:1.2:0.0, V/V), 20 min A/B/C (30:70:0,V/V), 30 min A/B/C (30:70:0, V/V), 30.1 min A/B/C (0:0:100, V/V), 46 min A/B/C (0:0:100, V/V), 46.1 min A/B/C (0:100:0, V/V), 50 min A/B/C (0:100:0, V/V), 50.1 min A/B/C (98.8:1.2:0.0, V/V) and 80 min A/B/C (98.8:1.2:0.0,V/V).

Polysaccharide infrared spectral detection. A total of 2 mg GLP and 200 mg potassium bromide were pressed into a pellet, with potassium bromide powder pressed into a pellet as a blank control. Fourier Transform Infrared Spectrometer FT-IR650 (Tianjin Gangdong Technology Development Co., Ltd.) was used for scanning and recording.

Blood biochemical profile assay. The levels of TC, TG, high-density lipoprotein cholesterol (HDL-C), LDL-C, estradiol (E2), INS, free fatty acid (FFA), alanine amino transferase (ALT) and aspartate aminotransferase (AST) in serum and fasting blood glucose (Roche Diabetes Care, Inc.; cat. nos. C8012 and P003874) were measured according to the manufacturer's protocols using kits [cat. nos. A111-1-1, A110-1-1, A112-1-1, A113-1-1 (all Nanjing Jiancheng Bioengineering Institute), MM-0546M1, MM-0579M1 and MM-0326M1 (all Meimian Bioengineering Company), C009-2-1 and C010-2-1 (both Nanjing Jiancheng Bioengineering Institute), respectively].

Hematoxylin and eosin (H&E) staining. The liver tissue was fixed in 4% paraformaldehyde at 4˚C overnight for histological staining. The 4-μm-thick paraffin sections were stained with hematoxylin (cat. no. H9627-100G) for 3 min and eosin (cat. no. E4009-25G; both Sigma-Aldrich; Merck KGaA) for 20 sec at room temperature. The images were captured with the Olympus DP74 light microscope and analyzed using Fijj (imagej.net/Contributors 2.14.0/1.54f).

Reverse transcription-quantitative (RT-q)PCR. Total RNA was obtained from each mouse liver using RNAiso plus reagent (cat. no. T9109, Takara Bio, Inc.) and subjected to RT using the Prime Script™ RT Reagent kit (cat. no. RR047A, Takara Bio, Inc.) at 37˚C for 15 min and 85˚C for 5 sec. qPCR was performed using the SYBR Premix Ex Taq kit (cat. no. RR820A, Takara Bio, Inc.) with the Light Cycler 480II System (Roche, Inc.). Thermocycling conditions were as follows: Initial denaturation at 95˚C for 30 sec, followed by 40 cycles of 95˚C for 5 sec, 60˚C for 20 sec and 65˚C for 15 sec. GAPDH was used as the internal reference. All primers used are listed in Table SI. Relative mRNA expression levels were calculated using the 2^−ΔΔCq method (35).

16S rDNA gene analysis. The feces of the mice were collected the day before tissue collection and stored in a -80˚C freezer. Then, fecal samples of 6 mice were randomly selected from each group for 16S rDNA sequencing. Gene Denovo Biotechnology Co., Ltd. performed the 16S rDNA high-throughput sequencing analysis. Genomic DNA was extracted using the HiPure Stool DNA kit (cat. no. D3141; Guangzhou Meiji Biotechnology Co., Ltd.). The quality and integrity of the processed DNA were verified using a NanoDrop 2000 micro-spectrophotometer (Thermo Fisher Scientific) to determine purity and by 2% agarose gel electrophoresis to confirm intact genomic DNA. The V3-V4 region of the 16S rDNA was amplified using primers as follows: forward, 5'-CCTACGGGNGGCWGC AG-3'; and reverse, 5'-GGACTACHVGGGTATCTAAT-3'. The purified amplification products were ligated to sequencing adapters to construct a sequencing library using the Illumina DNA Prep Kit (cat. no. 20060059; Illumina Inc.). PCR products were purified using AMPure XP Beads (Beckman Coulter) and quantified with a Qubit 3.0 fluorometer (Thermo Fisher Scientific). Library quality was validated using an ABI StepOnePlus Real-Time PCR System (Applied Biosystems). The pooled sequencing library (300 pM) was sequenced using the NovaSeq 6000 S2 Reagent Kit (cat. no. 20042038; Illumina Inc.) on an Illumina NovaSeq 6000 platform in paired-end 250 bp (PE250) mode. USEARCH (version 11.0.667; drive5.com/usearch/) was used for operational taxonomic unit clustering (97% similarity) with the UPARSE (version 11.0.667; drive5.com/uparse/) algorithm, UCHIME (version 11.0.667; drive5.com/usearch/manual/uchime_algo.html) for chimera removal, and the SILVA database (version 138.2; arb-silva.de/) for taxonomic annotation (36,37). Alpha diversity was assessed using the Shannon diversity index (38). Beta diversity was evaluated by principal coordinate analysis (PCoA) based on Bray-Curtis dissimilarity matrices (39,40). $H'=-\sum_{i=1}^{R} p_i \ln(p_i)$, where R is the total number of species (richness), and p_i is the proportion of individuals belonging to the i-th species. Higher Shannon values indicate greater diversity within the community. Functional prediction analysis. The functional profiles of the gut microbiota were predicted using PICRUSt2 based on the 16S rRNA gene sequencing data (41). The predicted functional pathways were annotated against the KEGG (Kyoto Encyclopedia of Genes and Genomes) database (42,43). Differential functional pathways between groups were identified using Statistical Analysis of Metagenomic Profiles; version 2.1.3) with two-sided Welch's t-test and Benjamini-Hochberg FDR correction ($q<0.05$) (44).

Western blotting. The liver tissues of the mice of each group were homogenized in RIPA lysis buffer (Dalian Meilun Biotechnology) and centrifuged (13,400 x g, 4˚C, 20 min) to collect the supernatant. Protein concentration was determined with a BCA assay kit. Aliquots (40 μg protein/lane) were resolved by 8-15% SDS-PAGE and transferred to PVDF membranes. Following blocking with 5% skimmed milk/TBST

(0.1% Tween-20, 1.5 h, room temperature), the membranes were probed with the primary antibodies (4˚C, overnight) followed by HRP-conjugated secondary antibodies (1 h, room temperature). Protein signals were visualized using ECL and quantified with ImageJ (v1.53k; National Institutes of Health). Antibody details are provided in Table SII. GAPDH, H3 and β-actin were used as internal controls.

Nuclear magnetic resonance (NMR) whole body composition analysis. The lean, fat mass, and liquid mass were assessed using a whole body composition analyzer (minispec LF90II; Bruker BioSpin). Conscious mice were placed into a plastic holder and inserted into the NMR magnet bore. Body composition was determined by time-domain nuclear magnetic resonance.

Statistical analysis. The experimental data were statistically analyzed and plotted using GraphPad Prism 8.0.2 (Dotmatics). One- or two-way repeated measures ANOVA was used to determine the differences between different groups, followed by Tukey's multiple comparisons post hoc test. $P<0.05$ was considered to indicate a statistically significant difference. All data are presented as the mean ± SEM. The experiments were independently repeated ≥3 times.

Results

GLP improves abnormal serum indexes and liver lipid accumulation of the OVX mice. GLP characterization was consistent with what is described in the literature (45) (Fig. S1). During the 8 weeks of the gavage, the OVX group showed a significantly faster rate of weight gain compared with the sham group. Pharmacological intervention moderated this weight gain, with all GLP-treated and the simvastatin group having significantly lower body weight than the OVX group (Figs. 1A and S2A). There was no significant difference in the average food intake of the mice in each group (Fig. S2B). Whole-body time-domain-NMR revealed that OVX group displayed the lowest lean mass and the highest fat mass across all groups (Fig. S2C and D). The lean mass of the OVX + HGLP group was increased relative to the OVX group (Fig. S2C). The fat mass of the OVX + MGLP group was decreased compared with the OVX group (Fig. S2D). The liquid mass of the OVX + HGLP group was decreased compared with the OVX group (Fig. S2E). Consistent with successful ovariectomy, serum E2 was markedly suppressed in every OVX group compared with Sham controls (Fig. 1B).

Serum lipid profiling showed that the LDL-C levels in mice of the OVX group increased compared with Sham controls. Serum LDL-C was decreased in the OVX + LGLP, MGLP and Siv groups compared with OVX group (Fig. 1C). In addition, HDL-C was upregulated in the HGLP and Siv groups compared with OVX group (Fig. 1C). The TC levels of the OVX group significantly increased compared with Sham group, and the TC levels of the OVX + LGLP, MGLP and Siv groups were decreased compared with OVX group (Fig. 1C). The TG levels increased in the OVX compared with Sham controls, and decreased in the OVX + LGLP, MGLP and Siv groups compared with the OVX group (Fig. 1C). Compared with the OVX group, the OVX + HGLP group showed a decrease in serum TC and TG levels although these were not significant (Fig. 1C). No inter-group differences were observed for ALT and AST (Fig. 1C). The FFA levels increased in the OVX group compared with the Sham controls, and decreased following administration of different doses of GLP or Siv (Fig. 1D). The levels of INS decreased in the OVX + HGLP group compared with the OVX group (Fig. 1D). There was no significant change in FBG between different groups (Fig. 1D).

The H&E staining confirmed that the OVX mice had more and larger lipid droplets in the liver, which demonstrated had liver fat accumulation, and HGLP significantly attenuated this lipid accumulation (Fig. 1E). Moreover, hepatic TC and TG were elevated in OVX compared with the Sham group, and the levels of TC in the livers of the OVX + MGLP and Siv groups were downregulated and the levels of TC and TG in the liver of the OVX + HGLP group were decreased compared with the OVX group (Fig. 1F).

GLP improves abnormal cholesterol synthesis of the OVX mice. Relative to Sham controls, hepatic sterol regulatory element binding transcription factor 2 (*Srebp2*) and 3-hydroxy-3-methylglutaryl-CoA reductase (*Hmgcr*) transcription was markedly elevated in the OVX group; this effect was decreased by GLP or Siv. The OVX + LGLP, MGLP and HGLP groups also showed effects similar to the OVX + Siv group in decreasing the transcription of *Srebp2* and *Hmgcr* (Fig. 2A). The mevalonate kinase (*Mvk*) mRNA was increased in OVX group compared with the Sham group, and this increase was decreased in the OVX + LGLP, HGLP and Siv groups (Fig. 2A). The diphosphomevalonate decarboxylase (*Mvd*) mRNA levels of the OVX + LGLP, HGLP and Siv groups were decreased compared with the OVX group (Fig. 2A). *Mvk* mRNA and protein changes in the OVX + MGLP group were not significant compared with the OVX + LGLP, HGLP and Siv groups (Fig. 2A). In addition, compared with the OVX group, only the OVX + HGLP group exhibited decreased transcription of farnesyl-diphosphate farnesyltransferase 1 and isopentenyl-diphosphate delta isomerase 1 (*Idi1*) (Fig. 2A). Hepatic farnesyl diphosphate synthase (*Fdps*) transcription in the OVX group was significantly upregulated compared with Sham controls, and this effect was decreased in the OVX + LGLP, HGLP and Siv groups. Compared with the OVX + Siv group, the OVX + MGLP group did not show significant transcriptional change of *Fdps* (Fig. 2A). The lanosterol synthase (*Lss*) mRNA expression decreased in the OVX + HGLP and Siv groups compared with the OVX group. There was no significant difference in transcript levels of *Lss* in the OVX + LGLP and MGLP groups (Fig. 2A). Compared with Sham controls, the expression of HMGCR protein in OVX mice was upregulated, and this change was reversed by MGLP, HGLP or Siv (Figs. 2B, C and S3A and B). LSS protein expression of the OVX group was increased compared with the Sham controls, and LSS protein expression of the OVX + HGLP group and Siv group was decreased compared with the OVX group (Fig. 2B and C). Hepatic MVK protein levels markedly increased in OVX mice compared with Sham controls, and were significantly attenuated following treatment with either HGLP or Siv (Figs. 2B, C and S3A and B). Hepatic IDI1 protein expression was markedly elevated in OVX mice relative to Sham controls and significantly reduced

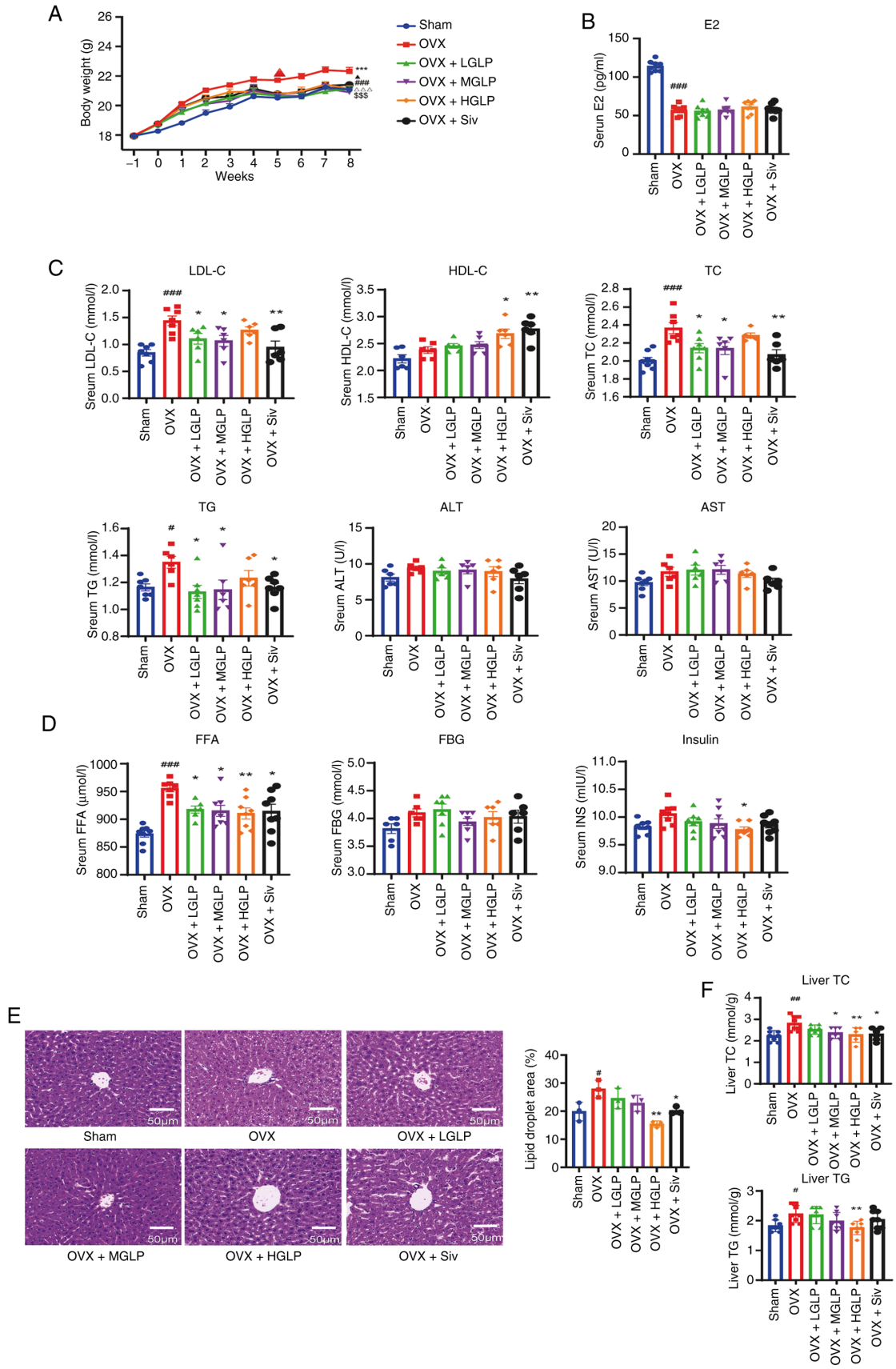

Figure 1. Effects of GLP on body weight, blood biochemical indexes and liver lipid content. (A) Body weight curves. ###P<0.005, Sham vs. OVX; ***P<0.005, OVX + LGLP vs. OVX; $$$P<0.005, OVX + MGLP vs. OVX; ΔΔΔP<0.005, OVX + HGLP vs. OVX; □P<0.05, OVX + Siv vs. OVX. Concentration of (B) E2 and (C) TG, TC, LDL-C, HDL-C, FFA, insulin and FBG in the serum. (D) Liver injury indexes including ALT and AST. (E) Hematoxylin and eosin staining and quantitative analysis of liver lipid droplet area of the liver tissue. Scale bar, 50 μm. (F) TG and TC content in the liver (n≥6). #P<0.05, ##P<0.01, ###P<0.005 vs. Sham; *P<0.05, **P<0.01 vs. OVX. GLP, *Ganoderma lucidum* polysaccharides; OVX, ovariectomy; LGLP, low-dose GLP; MGLP, medium-dose GLP; HGLP, high-dose GLP; Siv, simvastatin; E2, estradiol; LDL-C, low-density lipoprotein cholesterol; HDL-C, high-density lipoprotein cholesterol; TC, total cholesterol; TG, triglyceride; ALT, alanine aminotransferase; AST, aspartate transaminase; FFA, free fatty acid; FBG, fasting plasm glucose.

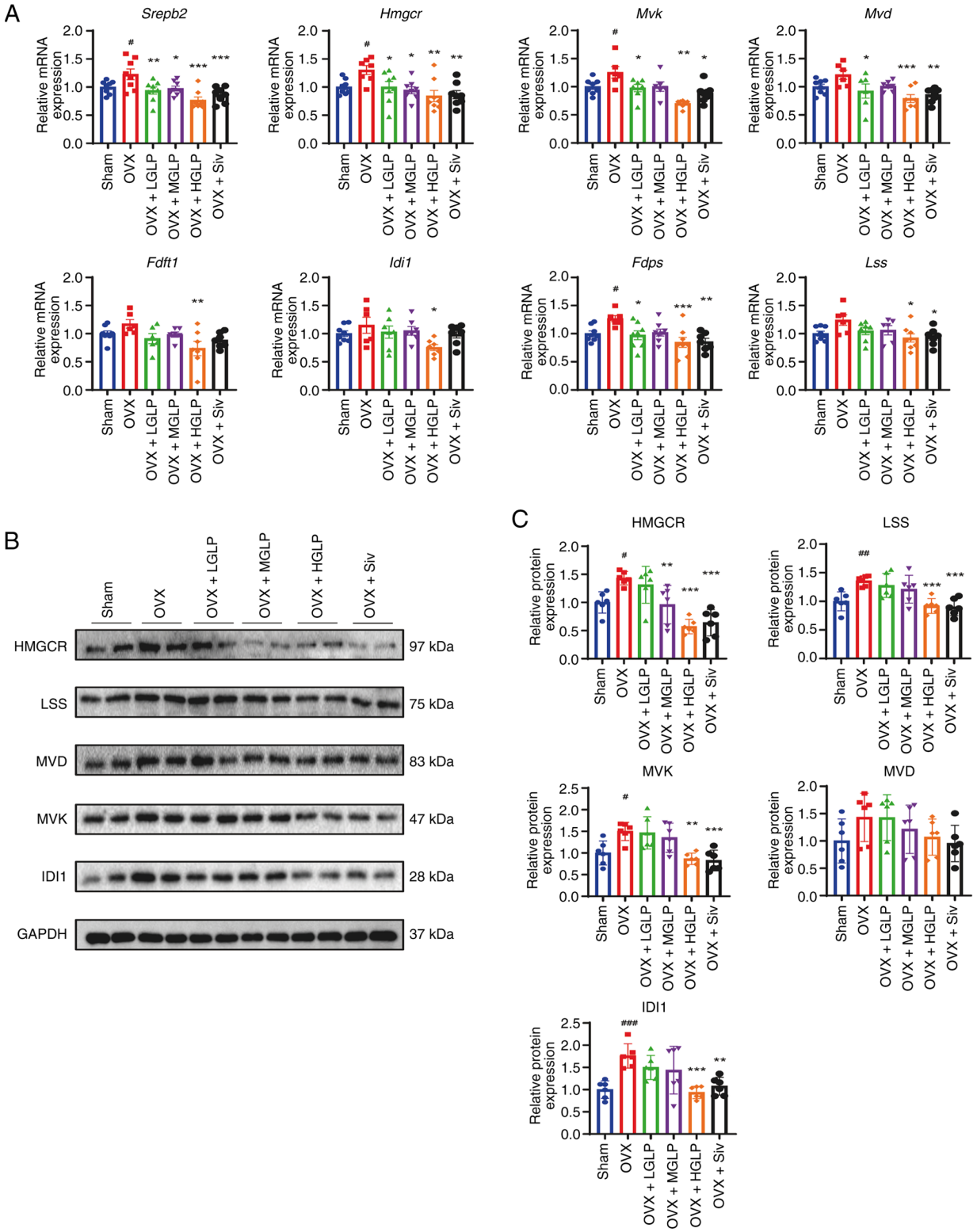

Figure 2. Effect of GLP on the expression of cholesterol synthesis-associated genes in the liver tissue. (A) Relative mRNA expression levels of *Srebp2*, *Hmgcr*, M*vk*, *Mvd*, *Fdft1*, *Idi1*, *Fdps* and *Lss* in the liver tissue. Protein levels detected by (B) western blot and (C) densitometry of HMGCR, LSS, MVK, MVD and IDI1 in the liver (n≥6). $^{\#}$P<0.05, $^{\#\#}$P<0.01, $^{\#\#\#}$P<0.005 vs. Sham; *P<0.05, **P<0.01, ***P<0.005 vs. OVX. GLP, *Ganoderma lucidum* polysaccharides; OVX, ovariectomy; LGLP, low-dose GLP; MGLP, medium-dose GLP; HGLP, high-dose GLP; Siv, simvastatin; Srebp2, sterol regulatory element-binding protein 2; Hmgcr, 3-hydroxy-3-methylglutaryl-coenzyme A reductase; Mvk, mevalonate kinase; Mvd, diphosphomevalonate decarboxylase; Fdft1, farnesyl-diphosphate farnesyltransferase 1; Idi1, isopentenyl-diphosphate delta isomerase 1; Fdps, farnesyl diphosphate synthase; Lss, lanosterol synthase.

by HGLP or Siv (Figs. 2B, C and S3A and B). MVD protein expression exhibited no marked variation between groups (Fig. 2B and C).

GLP downregulates hepatic transcription of FA biosynthetic enzymes in OVX mice. Hepatic *Srebp1-c* transcription of the OVX group was upregulated compared with the Sham controls,

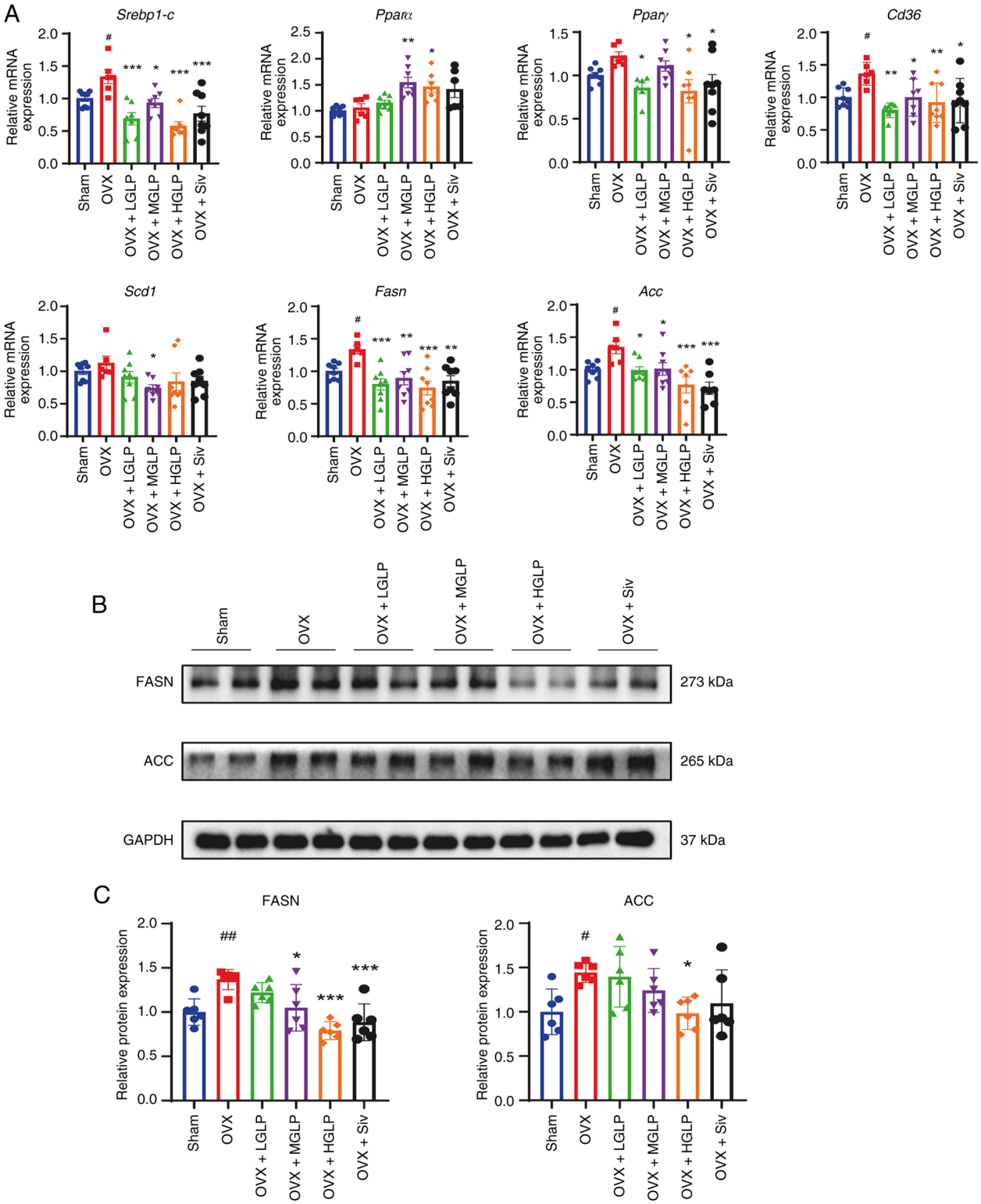

Figure 3. Effects of GLP on fatty acid synthesis of liver tissue. (A) mRNA expression of *Srebp1-c*, *Pparα*, *Pparγ*, *Cd36*, *Scd1*, *Fasn* and *Acc* at in the liver. (B) Western blotting and (C) densitometry of FASN and ACC in the liver (n≥6). $^{\#}$P<0.05, $^{\#\#}$P<0.01 vs. Sham; *P<0.05, **P<0.01, ***P<0.005 vs. OVX. GLP, *Ganoderma lucidum* polysaccharides; OVX, ovariectomy; LGLP, low-dose GLP; MGLP, medium-dose GLP; HGLP, high-dose GLP; Siv, simvastatin; Srebp1-c, sterol regulatory element-binding protein 1c; Pparα, peroxisome proliferator-activated receptor α; Scd1, stearoyl-CoA desaturase 1; Fasn, fatty acid synthase; Acc, acetyl CoA carboxylase.

and *Srebp1-c* mRNA expression was downregulated by all doses GLP or Siv (Fig. 3A). Peroxisome proliferator-activated receptor α (*Pparα*) mRNA was markedly elevated in the livers of the OVX + MGLP group and HGLP group compared with the OVX group (Fig. 3A). In addition, *Pparγ* transcription levels after treatment with LGLP, HGLP or Siv were significantly lower compared with the OVX group (Fig. 3A). The mRNA expression level of *Cd36* in the OVX mice was

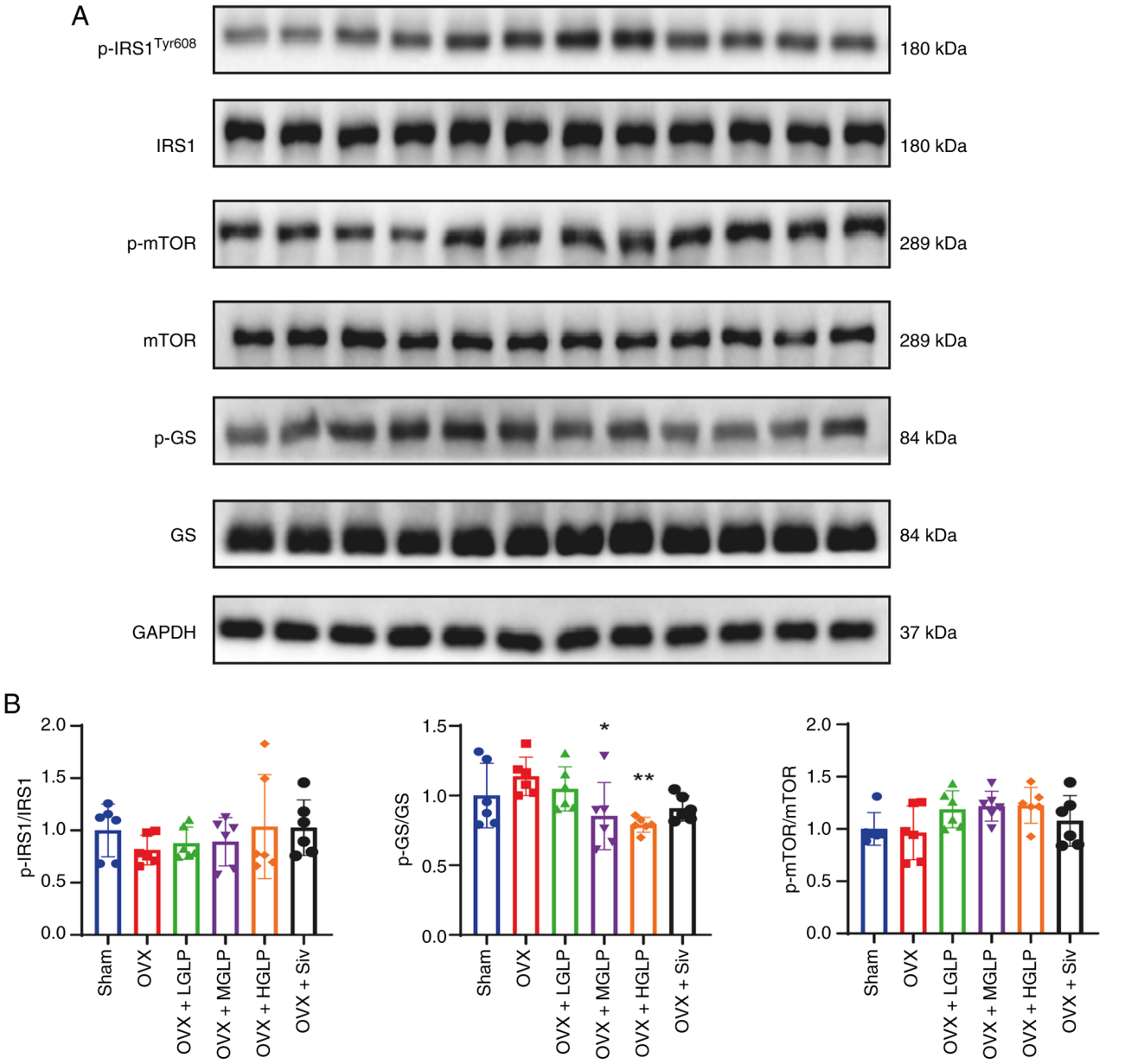

Figure 4. Effects of GLP on the expression of proteins involved in the insulin signaling pathway in the liver. (A) Expression of (B) p-IRS1, Tyr609, IRS1, p-mTOR, mTOR, p-GS and GS proteins in the liver (n≥6). *P<0.05, **P<0.01 vs. OVX. GLP, *Ganoderma lucidum* polysaccharides; OVX, ovariectomy; LGLP, low-dose GLP; MGLP, medium-dose GLP; HGLP, high-dose GLP; Siv, simvastatin; p-, phosphorylated; IRS1, insulin receptor substrate 1; GS, glycogen synthase.

increased compared with Sham controls. GLP and Siv reduced *Cd36* mRNA expression compared with the OVX group (Fig. 3A). The stearoyl-CoA desaturase 1 transcription level in the OVX + MGLP group was decreased compared with the OVX group (Fig. 3A). The *Fasn* and acetyl CoA carboxylase (*Acc*) mRNA expression levels in the mice of the OVX group were higher than the Sham controls, and this effect was decreased by all doses of GLP or Siv (Fig. 3A). FASN protein expression in the OVX group was increased compared with the Sham controls, and decreased in the OVX + MGLP, HGLP and Siv groups compared with OVX group (Fig. 3B and C). Hepatic ACC protein abundance was markedly elevated in OVX mice relative to Sham controls and was significantly attenuated by HGLP (Fig. 3B and C).

The ratio of phosphorylated (p-)glycogen synthase/glycogen synthase in the OVX + MGLP group and the HGLP group was significantly decreased compared with OVX group. There were no significant difference in the ratio of p-IRS1 (insulin receptor substrate (IRS1)/IRS1 and the ratio of p-mTOR/mTOR between groups (Fig. 4A and B).

GLP restores the abnormal expression of genes related to circadian rhythm in the OVX mice. Hepatic clock circadian regulator (*Clock*) transcription was significantly elevated in OVX + MGLP and HGLP livers relative to the OVX group (Fig. 5A). Basic helix-loop-helix ARNT like 1 (*Bmal1*) mRNA expression was markedly suppressed in the OVX group relative to Sham controls, and this change was restored by MGLP or HGLP (Fig. 5A). Hepatic period circadian regulator 1 transcription was significantly upregulated in OVX group relative to Sham controls, and administration of LGLP or HGLP effectively reversed this elevation (Fig. 5A). The *Per2* mRNA

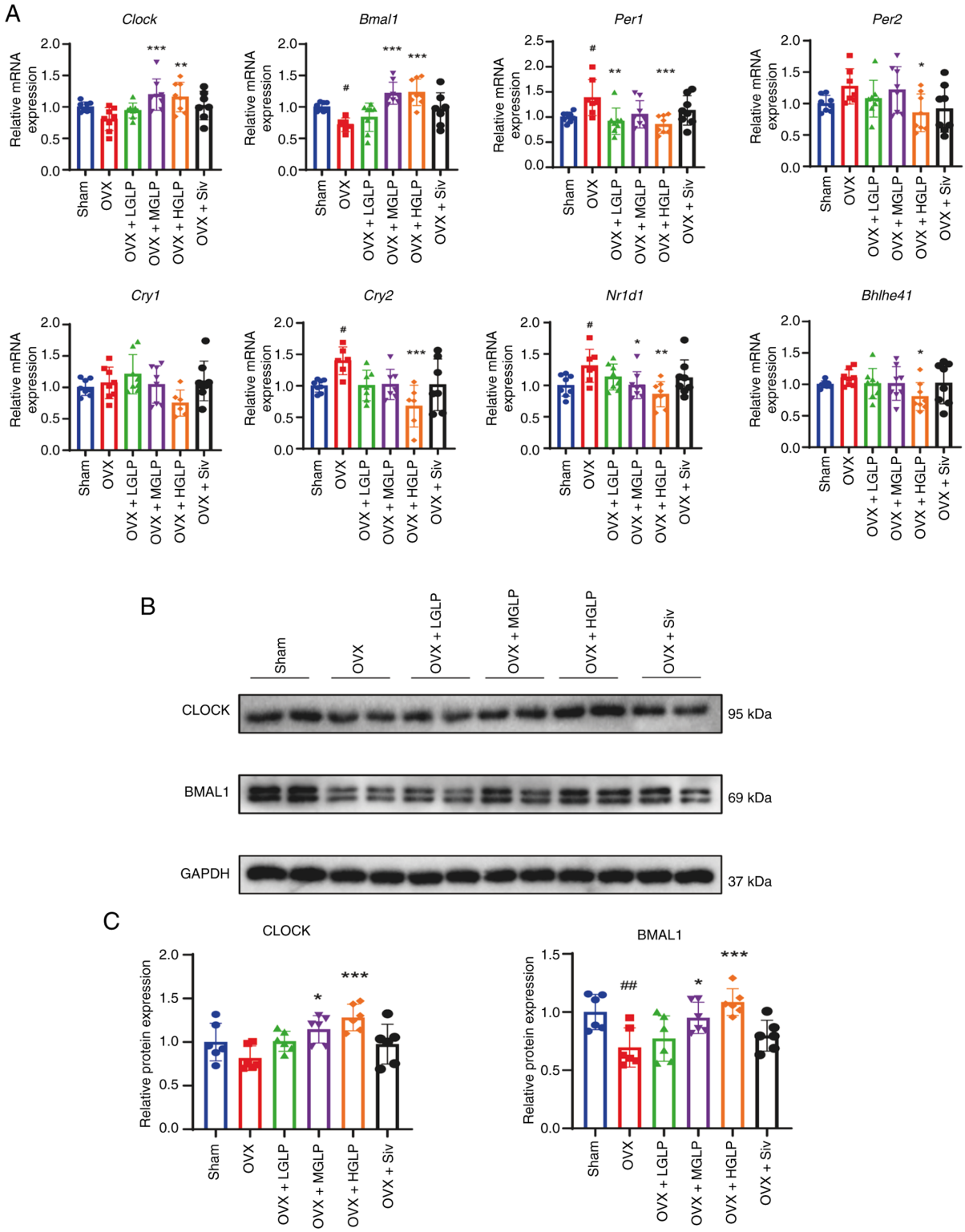

Figure 5. GLP improves the abnormal expression of genes associated with circadian rhythm. (A) mRNA expression levels of *Clock*, *Bmal1*, *Per1*, *Per2*, *Cry1*, *Cry2*, *Nr1d1* and *Bhlhe41* in the liver. (B) Protein expression levels of (C) CLOCK and BMAL1 in the liver. $^{\#}$P<0.05, $^{\#\#}$P<0.01 vs. Sham; *P<0.05, **P<0.01, ***P<0.005 vs. OVX. GLP, *Ganoderma lucidum* polysaccharides; OVX, ovariectomy; LGLP, low-dose GLP; MGLP, medium-dose GLP; HGLP, high-dose GLP; Siv, simvastatin; Bmal1, brain and muscle arnt-like protein 1; Per1, period circadian regulator 1; Cry1, cryptochrome circadian regulator 1; Nr1d1, nuclear receptor subfamily 1 group D member 1; Bhlhe41, basic helix-loop-helix family member e41.

of the OVX + HGLP group was downregulated relative to the OVX group (Fig. 5A). Cryptochrome circadian regulator 2 (*Cry2*) mRNA expression in the OVX group was increased compared with the Sham controls. However, compared with the OVX group, *Cry2* mRNA expression was decreased in the OVX + HGLP group (Fig. 5A). Nuclear receptor subfamily 1 group D member 1 (*Nr1d1*) mRNA expression in the OVX group was higher relative to Sham controls. Compared with the OVX group, the *Nr1d1* mRNA expression was reduced in the OVX + MGLP and HGLP groups (Fig. 5A). Basic

helix-loop-helix family member e41 (*Bhlhe41*) transcription in the OVX + HGLP group was lower than in the OVX group (Fig. 5A). As key regulators of the circadian rhythm (46), CLOCK and BMAL1 proteins were measured. Expression of CLOCK was increased in the OVX + MGLP group and HGLP group compared with the OVX group (Figs. 5B, C and S4A and B). The BMAL1 protein expression in the OVX group was decreased relative to Sham controls, and increased in the OVX + MGLP group and HGLP group compared with the OVX group (Figs. 5B, C and S4A and B).

GLP improves intestinal microbiota disorders of OVX mice. To explore the mechanism of GLP in improving the abnormal metabolism of lipids, the transcription of several genes associated with the estrogen receptor (ER) pathway was assessed. Compared with the OVX group, the mRNA expression of estrogen receptor 1 (*Esr1*), *Esr2*), HNF1 homeobox A (*Hnf1a*), and carnitine palmitoyltransferase 1A (*Cpt1a*) was significantly reduced in the OVX + Siv group. The mRNA expression of carnitine O-acetyltransferase (*Crat*) was significantly reduced in the OVX+ HGLP and Siv groups than the OVX group. The mRNA expression of family 27, subfamily a, polypeptide 1 (*Cyp27a1*) significantly increased in the OVX+HGLP group than the OVX group. The mRNA expression levels of the genes fatty acid desaturase 2 (*Fads2*), acyl-CoA synthetase long chain family member 5 (*Acsl5*), and ATP citrate lyase (*Acly*) showed no significant changes among the groups. Compared with the OVX group, the mRNA expression level of apolipoprotein A-II (*Apoa2*) was significantly increased in the OVX+LGLP group. The mRNA expression level of ATP binding cassette subfamily G member 8 (*Abcg8*) was significantly increased in the OVX+MGLP group than the OVX group. The mRNA expression of glycerol-3-phosphate acyltransferase, mitochondrial (*Gpam*) was significantly decreased in the OVX +LGLP, HGLP, and Siv groups compared with the OVX group (Fig. S5).

16S rDNA sequencing of the intestinal microbiota was performed. The Shannon diversity index of the OVX group showed an increase compared with the Sham group, while the Shannon diversity index of the OVX + HGLP group was decreased compared with the OVX group (Fig. 6A). PCoA showed that the microbiota of the OVX group was distinct from the Sham group indicating the structure of the microbiota was different between them, while the intestinal microbiota of the OVX + HGLP group was closer to that of the Sham group (Fig. 6B). The abundance of Verrucomicrobiota of the OVX + LGLP group was increased compared with the OVX group (Fig. S6). Abundance of *Akkermansia muciniphila* in the OVX + LGLP group was increased compared with the OVX group (Fig. 6C). Abundance of *Lactobacillus murinus* in the OVX + MGLP group was increased compared with the OVX group (Fig. 6C). There were 16 different bacterial groups between the OVX group and the Sham group: 12 bacterial groups were specific to the OVX group, including Verrucomicrobiota and Akkermansiaceae; the Sham group included four distinct bacterial groups, including *Alistipes* and *Muribaculum* (Fig. 6D). A total of 21 bacterial groups with differential abundance were detected between the OVX group and the OVX + HGLP group, and 15 bacterial groups, including Actinomycetota and lachnospiraceae_nk4a136_group, were identified as biomarkers enriched in the OVX group, moreover, there were six specific bacterial groups in the OVX + HGLP group, including *Allobaculum* and Erysipelatoclostridiaceae (Fig. 6E). Ovarian resection significantly enhanced the function of certain pathways compared with the Sham group, including 'amino acid metabolism', 'membrane transport', 'carbohydrate metabolism', 'cell motility', 'lipid metabolism', 'signal transduction' and 'metabolism of terpenoids and polyketides'. Compared with the OVX group, the functions of certain metabolic pathways of the OVX + LGLP group, HGLP and Siv groups were significantly inhibited, including 'carbohydrate metabolism', 'membrane transport', 'amino acid metabolism', 'cell motility', 'lipid metabolism', 'signal transduction', 'metabolism of terpenoids and polyketides', 'transcription', 'metabolism of cofactors and vitamins', 'energy metabolism', 'xenobiotics biodegradation and metabolism', 'biosynthesis of other secondary metabolites', 'cell growth and death', 'metabolism of other amino acids', 'replication and repair', 'nucleotide metabolism', 'folding, sorting and degradation', 'glycan biosynthesis and metabolism' and 'translation' (Fig. 6F).

Discussion

The present study treated OVX mice with L-, M- and HGLP for 8 weeks. GLP decreased the serum TC, TG and LDL-C levels, expression of genes associated with cholesterol and FA biosynthesis and lipid accumulation in the hepatic tissues of the OVX mice. Medium and high doses of GLP upregulate the expression of CLOCK and BMAL1 mRNA and protein, which are decreased due to ovariectomy. Finally, GLP influenced the intestinal microbiota disorder in mice caused by ovariectomy, regulated the intestinal microbial structure and increased the abundance of beneficial bacteria *A. muciniphila* and *L. murinus*.

With the onset of menopause, patients lack the protective effect of estrogen, resulting in changes in glucose and lipid metabolism; therefore, the risk of CVD increases, and by the age of 65 years, the incidence of CVD in female patients is the same as that in males (1,2,47). Moreover, the menopausal transition accelerates the accumulation of CVD risk factors, such as abdominal adiposity, INS resistance, arterial hypertension and atherogenic dyslipidemia including changes in serum LDL-C, TC, TG and apolipoprotein B (48). Two studies concluded that hormone therapy does not provide heart protection (2,49). Therefore, hormone therapy is not recommended to prevent primary or secondary cardiovascular disease and it is necessary to find more safe and effective drugs.

Polysaccharides serve a key role in metabolism by influencing lipid transport and distribution, regulating endogenous lipid synthesis and metabolism, inhibiting lipid peroxidation and affecting intestinal microbiota (12,50,51). GLP, the active component of *G. lucidum*, exhibits pharmacological characteristics in Traditional Chinese Medicine (52). For example, in a mouse model of diabetes, GLP shows a dose-dependent hypoglycemic effect, improving fasting blood glucose levels; the underlying mechanism may be associated with the activation of adenosine monophosphate-activated protein kinases and key glucose-metabolizing enzymes that regulate glycogenolysis or gluconeogenesis (53,54). Furthermore, GLP rectifies

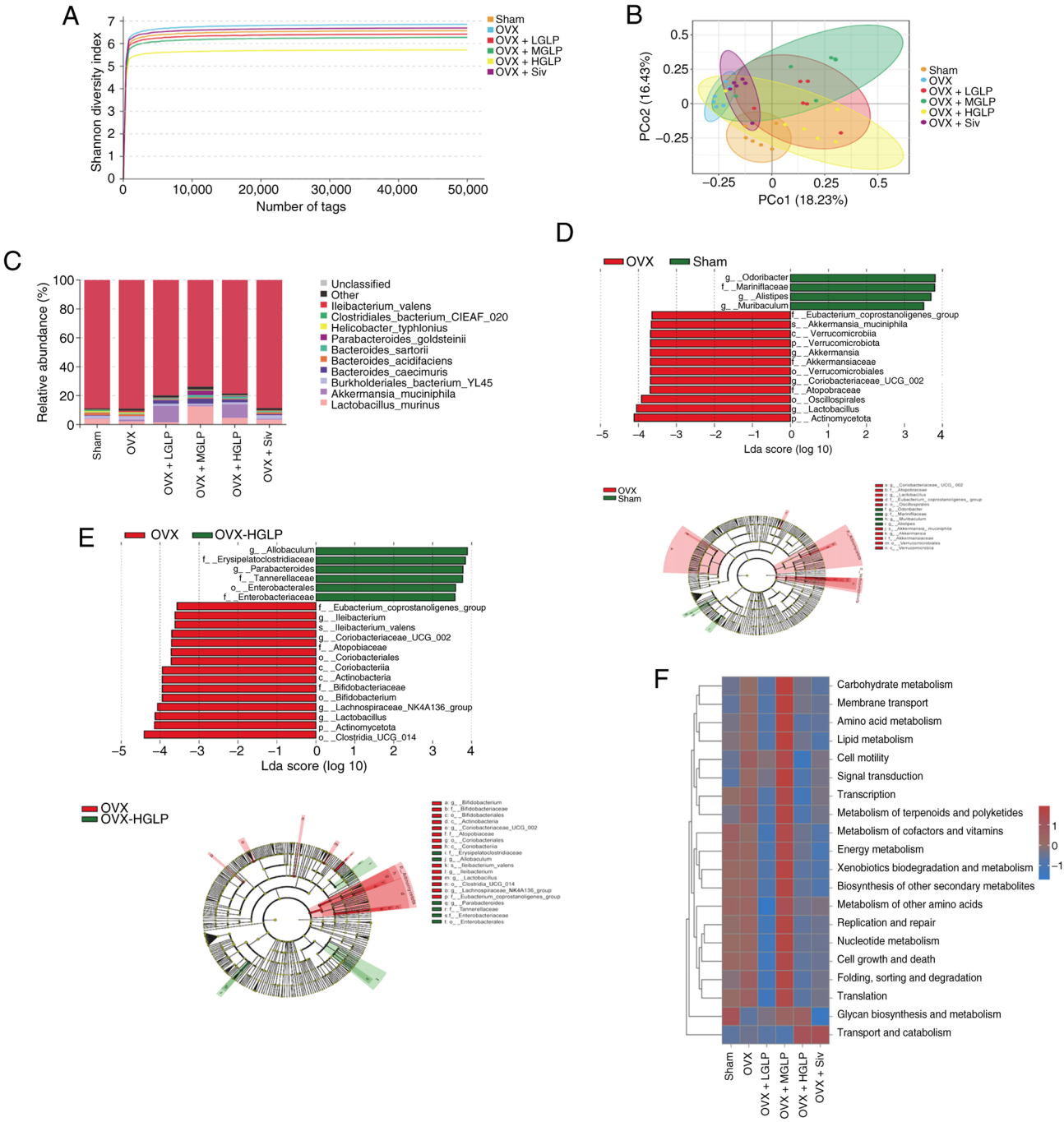

Figure 6. GLP improves intestinal microbiota of the OVX mice. (A) Shannon diversity index dilution curves. (B) PCo analysis community structure distribution. (C) Relative abundance of intestinal microbiota at the species level. Differential microbial community identification based on LDA effect size analysis of (D) Sham and (E) OVX + HGLP vs. OVX. (F) Signaling pathway enrichment analysis of the relative abundance of gut microbes (n=6). GLP, *Ganoderma lucidum* polysaccharides; OVX, ovariectomy; LGLP, low-dose GLP; MGLP, medium-dose GLP; HGLP, high-dose GLP; Siv, simvastatin; PCo, principal coordinate; LDA, linear discriminant analysis.

HFD-induced intestinal dysbiosis by decreasing the number of harmful bacteria while concomitantly suppressing pathobionts, thereby preserving gut-barrier integrity and attenuating metabolic endotoxemia (55). GLP decreases serum levels of TG, plasma TC and LDL-C and increase HDL-C levels, thereby regulating blood lipids and improving metabolic disorder (55,56). To the best of our knowledge, however, no studies have reported the role of GLP in regulating lipid metabolism in patients with declining ovarian function, and its specific role and mechanism need to be further explored. Here, GLP effectively decreased the weight gain and body fat content of the OVX mice. In dyslipidemia caused by ovarian resection, GLP may serve an ameliorating role, reducing the serum levels of LDL-C, TC, TG and FFA. HDL-C reverses transport of cholesterol and decreases excessive peripheral cholesterol accumulation (57). The present study demonstrated that HGLP could also increase serum HDL-C levels.

The liver, the key organ of material metabolism in the body, is responsible for regulating the metabolism of cholesterol and FAs. When intracellular cholesterol levels decrease,

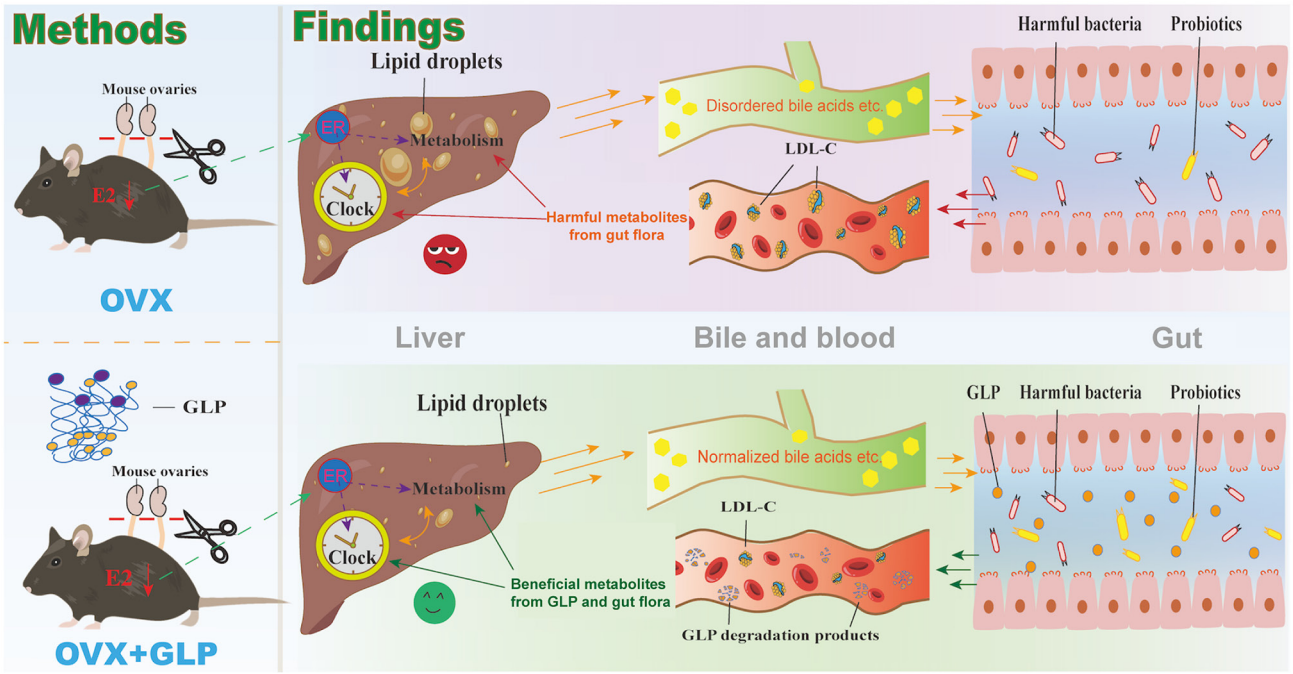

Figure 7. GLP improves liver metabolic disorder by modulating gut microbiota of OVX mice. GLPs upregulate the abundance of beneficial bacteria in the intestines of OVX mice, and then the metabolites produced by the beneficial bacteria and small molecules degraded from GLPs improve the lipid metabolic disorders and impaired circadian rhythm in the hepatic tissue of the OVX mice. GLP, *Ganoderma lucidum* polysaccharides; LDL-C, low-density lipoprotein cholesterol; OVX, ovariectomy.

Srebp2 is activated to enter the nucleus and initiate the expression of downstream genes associated with cholesterol synthesis to maintain cholesterol homeostasis (58). Hepatic *Srebp1-c* is a key transcription factor driving FA synthesis and *Pparγ* primarily promotes lipid storage and adipose tissue development; when these regulators of FA synthesis and storage are inhibited, FA synthesis and storage are decreased. *Pparα* mainly regulates FA oxidation, and its upregulation promotes metabolism of FAs (59). FASN and ACC are key enzymes in FA biosynthesis and their action forms the core engine of *de novo* lipogenesis, serving as a key hub connecting nutritional status with cellular lipid homeostasis (60). Hepatic steatosis is interrelated with insulin resistance; and insulin resistance, liver fibrosis, and gut-liver axis disorders are all key factors leading to the progression of MASLD (61-63). Here, GLP inhibited cholesterol synthesis in OVX mice by downregulating the expression of *Srebp2* and *Hmgcr*, key genes for cholesterol synthesis, at the mRNA level. In addition, GLP downregulated the mRNA expression of FA synthesis genes such as *Srebp1-c*, *Pparγ*, *Cd36*, *Fasn* and *Acc* and upregulated *Pparα* expression in the liver of the OVX mice. GLP regulates insulin signaling pathways and modulates FA metabolism through multiple mechanisms. Although these metabolism-related genes are regulated by the estrogen pathway, their expression levels are influenced by regulation from other pathways (64-66). However, the mRNA levels of most estrogen target genes showed no significant change in the liver tissues among the five groups. It was hypothesized that GLP may not primarily exert its effects through the estrogen pathway in the hepatic tissue. Moreover, within the peripheral circadian clock network, circadian rhythm genes are coupled to lipid, glucose and cholesterol homeostasis (67). Circadian rhythm disorder in the liver cause metabolic disorder, including metabolic disease such as hypertension, obesity and fatty liver disease (46,68,69), which threaten health. Here, ovariectomy downregulated the expression of *Clock* and *Bmal1*, while GLP increased the expression of *Clock* and *Bmal1* in OVX mice, thereby regulating circadian rhythm disorders.

GLP mitigates dextran sulfate sodium-induced colitis in rats by restructuring the colonic microbiota, moreover, GLP consumption regulated 11 genes, including six upregulated [C-C motif chemokine ligand 5 (*Ccl5*), CD3 epsilon subunit of T-cell receptor complex (*Cd3e*), CD8a molecule (*Cd8a*), interleukin 21 receptor (*Il21r*), lck proto-oncogene, Src family tyrosine kinase (*Lck*), and T cell receptor beta variable (*Trbv*)] and five downregulated [C-C motif chemokine ligand 3 (*Ccl3*), C-X-C motif chemokine ligand 1 (*Gro*), IL-11, major histocompatibility complex, class II (*Mhc2*), and prostaglandin-endoperoxide synthase (*Ptgs*)] genes resulting in enhancement of immunity and reduction of inflammatory response and colonic cancer risk (70). Ingestion of GLP reverses gut microbiota and metabolic disorder in rats with type 2 diabetes (25). The present results suggested GLP administration can effectively improve the richness and diversity of microbiota and regulate the composition of microbial communities following ovarian resection. *A. muciniphila* is a prominent member of Verrucomicrobiota; its depletion is associated with obesity, type 2 diabetes, hepatic steatosis and associated metabolic disorders (71), and it is a candidate next-generation probiotic. Levels of *A. muciniphila* in the intestine of obese and type 2 diabetic mice decrease, causing an imbalance of the intestinal microbiota; the abundance of *A. muciniphila* in the intestine is restored by supplementation with prebiotic preparations (72). In addition, therapeutic

supplementation with *A. muciniphila* reverses HFD-induced metabolic dysfunction, manifested as excess adiposity, metabolic endotoxemia, adipose tissue inflammation and INS resistance (72). Similarly, *L. murinus* improves glucose tolerance and INS sensitivity by enhancing FA oxidation (73). Here, GLP significantly affected the abundance of beneficial *A. muciniphila* and *L. murinus* bacteria in the intestinal tract of the OVX mice. Our previous correlation analysis between the gut microbiota of OVX mice and liver transcriptomes showed that Akkermansia is positively associated with *Cyp7a1*, while Lactobacillus is negatively associated with bile acid transport proteins [solute carrier family 10 (sodium/bile acid cotransporter family), member 1 (*Ntcp*), ATP-binding cassette, sub-family B member 11 (*Bsep*)], which also supports that the hypothesis that the mechanism of GLP may partially involve the gut-liver axis (74). Therefore, GLP may improve liver lipid metabolism disorder caused by decreased ovarian function by increasing the abundance of gut probiotics and partially acting through the gut-liver axis. Due to the experimental design, the present study did not explore the causal association between GLP and the gut-liver axis in depth, and lacked correlation analysis between specific microbial populations and key metabolic parameters, as well as functional metagenomics and fecal microbiota transplantation experiments.

In summary, GLP influences the structure of the gut microbiota and increases the abundance of probiotics (Fig. 7), thereby improving liver glucose and lipid metabolic disorder caused by decreased or absent ovarian function. The present study demonstrated that GLP and Siv have similar effects in improving liver lipid metabolism in OVX mice, indicating that GLP has certain potential for the prevention and treatment of lipid metabolic disorder in menopausal patients. However, GLP offers distinct clinical advantages over Siv. Siv primarily inhibits 3-hydroxy-3-methylglutaryl-Coenzyme A reductase (75). Compared with Siv, GLP is more effective at increasing the proportion of probiotics, such as *A. muciniphila*. Since GLP is not easily absorbed by the gut, it acts directly on the intestinal microbiota, enhancing the structure and function of the microbiome, which may regulate liver glucose and lipid metabolism through the gut-liver axis. As a natural plant polysaccharide, GLP may have a superior safety profile and tolerability compared with statins, which are associated with myopathy, hepatotoxicity and new-onset diabetes (76-78). This renders GLP suitable for long-term preventive use in postmenopausal patients with dyslipidemia and metabolic comorbidities. Furthermore, the distinct mechanisms suggest potential for combination therapy, where GLP could enhance statin efficacy while mitigating adverse effects. As a natural product, GLP may also offer cost-effectiveness advantages. Collectively, GLP matches Siv in lipid-lowering efficacy while providing added value through its microbiota-centered benefits and favorable safety profile, positioning it as a candidate for managing postmenopausal metabolic disorder. In addition, GLP can also affect the expression of hepatic circadian rhythm genes, thereby influencing glucose and lipid metabolism in the liver by modulating the expression of genes associated with these metabolic processes. Given the high incidence of cardiovascular disease in elderly patients, GLP has potential efficacy in treating metabolic disorder caused by decreased ovarian function.

Acknowledgements

Not applicable.

Funding

The present study was supported by the National Natural Science Foundation of China (grant no. 82171855) and the Key Field Special Project for Colleges and Universities of Guangdong Province (Biomedicine and Health; grant no. 2023ZDZX2030).

Availability of data and materials

The data generated in the present study may be found in the Sequence read archive under accession no. PRJNA1279352 or at the following URL: https://www.ncbi.nlm.nih.gov/bioproject/PRJNA1279352.

Authors' contributions

XJ conceived and designed the study and analyzed data. XL analyzed data, constructed figures and wrote the manuscript. YJW designed the experiments. ZLL and YHY conceived the study, performed the experiments and edited the manuscript. XJ and XL confirm the authenticity of all the raw dat. All authors have read and approved the final manuscript.

Ethics approval and consent to participate

All the animal experiments were approved by the Experimental Animal Ethics Committee of Guangdong Pharmaceutical University (Guangzhou, China; approval no. gdpulac2020065).

Patient consent for publication

Not applicable.

Competing interests

The authors declare that they have no competing interests.

References

1. Gatenby C and Simpson P: Menopause: Physiology, definitions, and symptoms. Best Pract Res Clin Endocrinol Metab 38: 101855, 2024.
2. Gersh FL, O'Keefe JH and Lavie CJ: Postmenopausal hormone therapy for cardiovascular health: The evolving data. Heart 107: 1115-1122, 2021.
3. Li H, Sun R, Chen Q, Guo Q, Wang J, Lu L and Zhang Y: Association between HDL-C levels and menopause: A meta-analysis. Hormones (Athens) 20: 49-59, 2021.
4. Chen Y, Wang A, Zhang X, Xia F and Zhao X: Effect of age at menopause and menopause itself on high sensitivity C-reactive protein, pulse wave velocity, and carotid intima-media thickness in a Chinese population. Medicine (Baltimore) 102: e35629, 2023.
5. Witteman JC, Grobbee DE, Kok FJ, Hofman A and Valkenburg HA: Increased risk of atherosclerosis in women after the menopause. BMJ 298: 642-644, 1989.
6. Zaydun G, Tomiyama H, Hashimoto H, Arai T, Koji Y, Yambe M, Motobe K, Hori S and Yamashina A: Menopause is an independent factor augmenting the age-related increase in arterial stiffness in the early postmenopausal phase. Atherosclerosis 184: 137-142, 2006.

7. Colditz GA, Willett WC, Stampfer MJ, Rosner B, Speizer FE and Hennekens CH: Menopause and the risk of coronary heart disease in women. N Engl J Med 316: 1105, 1987.
8. Talaulikar V: Menopause transition: Physiology and symptoms. Best Pract Res Clin Obstet Gynaecol 81: 3-7, 2022.
9. Lee E, Anselmo M, Tahsin CT, Vanden Noven M, Stokes W, Carter JR and Keller-Ross ML: Vasomotor symptoms of menopause, autonomic dysfunction, and cardiovascular disease. Am J Physiol Heart Circ Physiol 323: H1270-H1280, 2022.
10. Liu Y and Li C: Hormone therapy and biological aging in postmenopausal women. JAMA Netw Open 7: e2430839, 2024.
11. Innes KE, Selfe TK and Vishnu A: Mind-body therapies for menopausal symptoms: A systematic review. Maturitas 66: 135-149, 2010.
12. Yu Y, Shen M, Song Q and Xie J: Biological activities and pharmaceutical applications of polysaccharide from natural resources: A review. Carbohydr. Polym 183: 91-101, 2018.
13. Cao Y, Xu X, Liu S, Huang L and Gu J: *Ganoderma*: A cancer immunotherapy review. Front Pharmacol 9: 1217, 2018.
14. Zhang J, Liu Y, Tang Q, Zhou S, Feng J and Chen H: Polysaccharide of *Ganoderma* and its bioactivities. Adv Exp Med Biol 1181: 107-134, 2019.
15. Zhou Y, Wang M, Wang Z, Qiu J, Wang Y, Li J, Dong F, Huang X, Zhao J and Xu T: Polysaccharides from hawthorn fruit alleviate high-fat diet-induced NAFLD in mice by improving gut microbiota dysbiosis and hepatic metabolic disorder. Phytomedicine 139: 156458, 2025.
16. Shiao MS: Natural products of the medicinal fungus *Ganoderma lucidum*: occurrence, biological activities, and pharmacological functions. Chem Rec 3: 172-180, 2003.
17. Sohretoglu D and Huang S: *Ganoderma lucidum* polysaccharides as an anti-cancer agent. Anticancer Agents Med Chem 18: 667-674, 2018.
18. Seweryn E, Ziała A and Gamian A: Health-promoting of polysaccharides extracted from *Ganoderma lucidum*. Nutrients 13: 2725, 2021.
19. Li J, Niu D, Zhang Y and Zeng XA: Physicochemical properties, antioxidant and antiproliferative activities of polysaccharides from Morinda citrifolia L. (Noni) based on different extraction methods. Int J Biol Macromol 150: 114-121, 2020.
20. Zeng P, Guo Z, Zeng X, Hao C, Zhang Y, Zhang M, Liu Y, Li H, Li J and Zhang L: Chemical, biochemical, preclinical and clinical studies of *Ganoderma lucidum* polysaccharide as an approved drug for treating myopathy and other diseases in China. J Cell Mol Med 22: 3278-3297, 2018.
21. Li Y, Tang J, Gao H, Xu Y, Han Y, Shang H, Lu Y and Qin C: *Ganoderma lucidum* triterpenoids and polysaccharides attenuate atherosclerotic plaque in high-fat diet rabbits. Nutr Metab Cardiovasc Dis 31: 1929-1938, 2021.
22. Vitak T, Yurkiv B, Wasser S, Nevo E and Sybirna N: Effect of medicinal mushrooms on blood cells under conditions of diabetes mellitus. World J Diabetes 8: 187-201, 2017.
23. Zheng Y, Bai L, Zhou Y, Tong R, Zeng M, Li X and Shi J: Polysaccharides from Chinese herbal medicine for anti-diabetes recent advances. Int J Biol Macromol 121: 1240-1253, 2019.
24. Sang T, Guo C, Guo D, Wu J, Wang Y, Wang Y, Chen J, Chen C, Wu K, Na K, *et al*: Suppression of obesity and inflammation by polysaccharide from sporoderm-broken spore of *Ganoderma lucidum* via gut microbiota regulation. Carbohydr Polym 256: 117594, 2021.
25. Chen M, Xiao D, Liu W, Song Y, Zou B, Li L, Li P, Cai Y, Liu D, Liao Q and Xie Z: Intake of *Ganoderma lucidum* polysaccharides reverses the disturbed gut microbiota and metabolism in type 2 diabetic rats. Int J Biol Macromol 155: 890-902, 2020.
26. Baker JM, Al-Nakkash L and Herbst-Kralovetz MM: Estrogen-gut microbiome axis: Physiological and clinical implications. Maturitas 103: 45-53, 2017.
27. Yang M, Wen S, Zhang J, Peng J, Shen X and Xu L: Systematic review and meta-analysis: Changes of gut microbiota before and after menopause. Dis Markers 2022: 3767373, 2022.
28. Liu Y, Zhou Y, Mao T, Huang Y, Liang J, Zhu M, Yao P, Zong Y, Lang J and Zhang Y: The relationship between menopausal syndrome and gut microbes. BMC Womens Health 22: 437, 2022.
29. Pavlovska OM, Pavlovska KM, Heryak SM, Khmil SV and Khmil MS: Vasomotor menopausal disorders as a possible result of dysfunction of the microbiota-intestine-brain axis. J Med Life 15: 234-240, 2022.
30. Hu S, Ding Q, Zhang W, Kang M, Ma J and Zhao L: Gut microbial beta-glucuronidase: A vital regulator in female estrogen metabolism. Gut Microbes 15: 2236749, 2023.
31. Trefts E, Gannon M and Wasserman DH: The liver: Curr Biol 27: R1147-R1151, 2017.
32. Guo X, Okpara ES, Hu W, Yan C, Wang Y, Liang Q, Chiang JYL and Han S: Interactive relationships between intestinal flora and bile acids. Int J Mol Sci 23: 8343, 2022.
33. Liu S and Yang X: Intestinal flora plays a role in the progression of hepatitis-cirrhosis-liver cancer. Front Cell Infect Microbiol 13: 1140126, 2023.
34. Lilley E, Stanford SC, Kendall DE, Alexander SPH, Cirino G, Docherty JR, George CH, Insel PA, Izzo AA, Ji Y, *et al*: ARRIVE 2.0 and the British journal of pharmacology: Updated guidance for 2020. Br J Pharmacol 177: 3611-3616, 2020.
35. Livak KJ and Schmittgen TD: Analysis of relative gene expression data using real-time quantitative PCR and the 2(-Delta Delta C(T)) method. Methods 25: 402: 408, 2001.
36. Edgar RC: Search and clustering orders of magnitude faster than BLAST. Bioinformatics 26: 2460-2461, 2010.
37. Edgar RC, Haas BJ, Clemente JC, Quince C and Knight R: UCHIME improves sensitivity and speed of chimera detection. Bioinformatics 27: 2194-2200, 2011.
38. Shannon CE: A mathematical theory of communication. Bell Syst Tech J 27: 379-423, 623-656, 1948.
39. Gower JC: Some distance properties of latent root and vector methods used in multivariate analysis. Biometrika 53: 325-338, 1966.
40. Bray JR and Curtis JT: An ordination of the upland forest communities of southern wisconsin. Ecol Monogr 27: 325-349, 1957.
41. Douglas GM, Maffei VJ, Zaneveld JR, Yurgel SN, Brown JR, Taylor CM, Huttenhower C and Langille MGI: PICRUSt2 for prediction of metagenome functions. Nat Biotechnol 38: 685-688, 2020.
42. Kanehisa M and Goto S: KEGG: Kyoto encyclopedia of genes and genomes. Nucleic Acids Res 28: 27-30, 2000.
43. Kanehisa M, Goto S, Sato Y, Kawashima M, Furumichi M and Tanabe M: Data, information, knowledge and principle: Back to metabolism in KEGG. Nucleic Acids Res 42 (Database Issue): D199-D205, 2014.
44. Parks DH, Tyson GW, Hugenholtz P and Beiko RG: STAMP: Statistical analysis of taxonomic and functional profiles. Bioinformatics 30: 3123-3124, 2014.
45. Liang XL, Liang YW, Tian J, Mo FF, Pan TM, Chen YF, Shao XQ and Li KP: Structural characterization and oxidative stress modulation activity of an acidic Heteropolysaccharide from Microctis folium. Carbohydr Polym 369: 124261, 2025.
46. Reppert SM and Weaver DR: Coordination of circadian timing in mammals. Nature 418: 935-941, 2002.
47. Otto CM: Heartbeat: Is postmenopausal hormone therapy a risk factor or preventative therapy for cardiovascular disease in women? Heart 107: 1103-1105, 2021.
48. Anagnostis P and Stevenson JC: Cardiovascular health and the menopause, metabolic health. Best Pract Res Clin Endocrinol Metab 38: 101781, 2024.
49. Rossouw JE, Anderson GL, Prentice RL, LaCroix AZ, Kooperberg C, Stefanick ML, Jackson RD, Beresford SA, Howard BV, Johnson KC, *et al*: Risks and benefits of estrogen plus progestin in healthy postmenopausal women: Principal results from the women's health initiative randomized controlled trial. JAMA 288: 321-333, 2002.
50. Nai J, Zhang C, Shao H, Li B, Li H, Gao L, Dai M, Zhu L and Sheng H: Extraction, structure, pharmacological activities and drug carrier applications of Angelica sinensis polysaccharide. Int J Biol Macromol 183: 2337-2353, 2021.
51. Fang S, Wang T, Li Y, Xue H, Zou J, Cai J, Shi R, Wu J and Ma Y: Gardenia jasminoides Ellis polysaccharide ameliorates cholestatic liver injury by alleviating gut microbiota dysbiosis and inhibiting the TLR4/NF-κB signaling pathway. Int J Biol Macromol 205: 23-36, 2022.
52. Ahmad R, Riaz M, Khan A, Aljamea A, Algheryafi M, Sewaket D and Alqathama A: *Ganoderma lucidum* (Reishi) an edible mushroom; a comprehensive and critical review of its nutritional, cosmeceutical, mycochemical, pharmacological, clinical, and toxicological properties. Phytother Res 35: 6030, 2021.
53. Xiao C, Wu QP, Cai W, Tan JB, Yang XB and Zhang JM: Hypoglycemic effects of *Ganoderma lucidum* polysaccharides in type 2 diabetic mice. Arch Pharm Res 35: 1793-1801, 2012.
54. Xiao C, Wu Q, Zhang J, Xie Y, Cai W and Tan J: Antidiabetic activity of *Ganoderma lucidum* polysaccharides F31 down-regulated hepatic glucose regulatory enzymes in diabetic mice. J Ethnopharmacol 196: 47-57, 2017.

55. Chang CJ, Lin CS, Lu CC, Martel J, Ko YF, Ojcius DM, Tseng SF, Wu TR, Chen YY, Young JD and Lai HC: *Ganoderma lucidum* reduces obesity in mice by modulating the composition of the gut microbiota. Nat Commun 6: 7489, 2015.
56. Zhu K, Nie S, Li C, Lin S, Xing M, Li W, Gong D and Xie M: A newly identified polysaccharide from *Ganoderma* atrum attenuates hyperglycemia and hyperlipidemia. Int J Biol Macromol 57: 142-150, 2013.
57. Jung E, Kong SY, Ro YS, Ryu HH and Shin SD: Serum cholesterol levels and risk of cardiovascular death: A systematic review and a dose-response meta-analysis of prospective cohort studies. Int J Environ Res Public Health 19: 8272, 2022.
58. Xiao MY, Pei WJ, Li S, Li FF, Xie P, Luo HT, Hyun Yoo H and Piao XL: Gypenoside L inhibits hepatocellular carcinoma by targeting the SREBP2-HMGCS1 axis and enhancing immune response. Bioorg Chem 150: 107539, 2024.
59. Zhao R, Chen Q and He YM: The effect of *Ganoderma lucidum* extract on immunological function and identify its anti-tumor immunostimulatory activity based on the biological network. Sci Rep 8: 12680, 2018.
60. Yu W, Qiu J, Chen Y, Che X and Li X: Chrysanthemum morifolium extract improves metabolic dysfunction-associated fatty liver disease by regulating lipid metabolism. Sci Rep 15: 40069, 2025.
61. Romanos M, Garcia Cordova JM, Villamarin J, Pazmino Zurita JD and Acosta A: Obesity and metabolic dysfunction-associated steatotic liver disease (MASLD): A literature review on pathophysiology and treatment. Diabetes Obes Metab 28 (Suppl2): S19-S30, 2026.
62. Cuthbertson DJ, Whyte M, Henney AE, Alam U, Goff L, Fielding BA and Umpleby AM: Differential pathophysiological drivers of susceptibility to type 2 diabetes and metabolic dysfunction-associated steatotic liver disease: Ethnic differences in insulin dynamics, whole-body fat metabolism, and organ-specific lipid deposition. Obes Rev 2026: e70104, 2026.
63. Servin-Uribe RI, Pérez-Jiménez J, Castaño Tostado E, Hernández-Saavedra D and Reynoso Camacho R: Hepatic lipids as molecular targets in obesity-associated insulin resistance in rodent models: A systematic review and meta-analysis. Lipids: Apr 28, 2026 (Epub ahead of print).
64. Fuentes N and Silveyra P: Estrogen receptor signaling mechanisms. Adv Protein Chem Struct Biol 116: 135-170, 2019.
65. MacLeod B, Wang C, Brown LH, Borkowski E, Nakamura MT, Wells KR, Brunt KR, Harasim-Symbor E, Chabowski A and Mutch DM: Fads2 knockout mice reveal that ALA prevention of hepatic steatosis is dependent on delta-6 desaturase activity. J Lipid Res 65: 100642, 2024.
66. Li Z, Zheng D, Zhang T, Ruan S, Li N, Yu Y, Peng Y and Wang D: The roles of nuclear receptors in cholesterol metabolism and reverse cholesterol transport in nonalcoholic fatty liver disease. Hepatol Commun 8: e0343, 2023.
67. Tseng HL, Yang SC, Yang SH and Shieh KR: Hepatic circadian-clock system altered by insulin resistance, diabetes and insulin sensitizer in mice. PLoS One 10: e0120380, 2015.
68. Eckel-Mahan K and Sassone-Corsi P: Metabolism control by the circadian clock and vice versa. Nat Struct Mol Biol 16: 462-467, 2009.
69. Gachon F, Bugianesi E, Castelnuovo G, Oster H, Pendergast JS and Montagnese S: Potential bidirectional communication between the liver and the central circadian clock in MASLD. NPJ Metab Health Dis 3: 15, 2025.
70. Xie J, Liu Y, Chen B, Zhang G, Ou S, Luo J and Peng X: *Ganoderma lucidum* polysaccharide improves rat DSS-induced colitis by altering cecal microbiota and gene expression of colonic epithelial cells. Food Nutr Res 63: 10.29219/fnr.v63.1559, 2019.
71. Cani PD, Depommier C, Derrien M, Everard A and de Vos WM: *Akkermansia muciniphila*: Paradigm for next-generation beneficial microorganisms. Nat Rev Gastroenterol Hepatol 19: 625-637, 2022.
72. Everard A, Belzer C, Geurts L, Ouwerkerk JP, Druart C, Bindels LB, Guiot Y, Derrien M, Muccioli GG, Delzenne NM, *et al*: Cross-talk between *Akkermansia muciniphila* and intestinal epithelium controls diet-induced obesity. Proc Natl Acad Sci USA 110: 9066-9071, 2013.
73. Long J, Shi Z, Miao Z, Dong L and Yan D: *Lactobacillus murinus* alleviates insulin resistance via promoting L-citrulline synthesis. J Endocrinol Invest 48: 1005-1015, 2025.
74. Jin X, Liu X, Wang Y, Li X, Zhang T, Li J, Lei Z and Yang Y: The mechanism by which melatonin improves the dysregulation of glucose and lipid metabolism in castrated female mice. J Pineal Res 77: e70082, 2025.
75. Lennernäs H and Fager G: Pharmacodynamics and pharmacokinetics of the HMG-CoA reductase inhibitors. Similarities and differences. Clin Pharmacokinet 32: 403-425, 1997.
76. Ramsey LB, Johnson SG, Caudle KE, Haidar CE, Voora D, Wilke RA, Maxwell WD, McLeod HL, Krauss RM, Roden DM, *et al*: The clinical pharmacogenetics implementation consortium guideline for SLCO1B1 and simvastatin-induced myopathy: 2014 update. Clin Pharmacol Ther 96: 423-428, 2014.
77. Zhou L, Wu B, Bian Y, Lu Y, Zou Y, Lin S, Li Q and Liu C: Hepatotoxicity associated with statins: A retrospective pharmacovigilance study based on the FAERS database. PLoS One 20: e0327500, 2025.
78. Wang X, Li J, Wang T, Zhang Z, Li Q, Ma D, Chen Z, Ju J, Xu H and Chen K: Associations between statins and adverse events in secondary prevention of cardiovascular disease: Pairwise, network, and dose-response meta-analyses of 47 randomized controlled trials. Front Cardiovasc Med 9: 929020, 2022.